AGU PUBLICATIONS

JGR

Journal of Geophysical Research: Atmospheres

RESEARCH ARTICLE
10.1002/2016JD025144

Global observations of 2 day wave coupling to the diurnal tide in a high-altitude forecast-assimilation system

R. S. Lieberman[1], D. M. Riggin[1], V. Nguyen[2], S. E. Palo[2], D. E. Siskind[3], N. J. Mitchell[4], G. Stober[5], S. Wilhelm[5], and N. J. Livesey[6]

[1]GATS Inc., Boulder, Colorado, USA, [2]Department of Aerospace Engineering Sciences, University of Colorado Boulder, Boulder, Colorado, USA, [3]Space Science Division, Naval Research Laboratory, Washington, District of Columbia, USA, [4]Department of Electronic and Electrical EngineeringUniversity of Bath, Bath, UK, [5]Leibniz Institute of Atmospheric Physics, University of Rostock, Kühlungsborn, Germany, [6]Jet Propulsion Laboratory, California Institute of Technology, Pasadena, California, USA

Key Points:
- We have identified diurnal tide-2 day wave interaction products in a global middle atmosphere data set
- We have confirmed nonlinear interaction as a source using a numerical model with realistic background winds and temperatures
- We have compared the westward traveling 16 h wave with ground-based radar wind measurements

Correspondence to:
R. S. Lieberman,
rlieberm@nsf.gov

Citation:
Lieberman, R. S., D. M. Riggin, V. Nguyen, S. E. Palo, D. E. Siskind, N. J. Mitchell, G. Stober, S. Wilhelm, and N. J. Livesey (2017), Global observations of 2 day wave coupling to the diurnal tide in a high-altitude forecast-assimilation system, *J. Geophys. Res. Atmos.*, *122*, 4135–4149, doi:10.1002/2016JD025144.

Received 24 MAR 2016
Accepted 21 MAR 2017
Accepted article online 23 MAR 2017
Published online 18 APR 2017

Abstract We examine wave components in a high-altitude forecast-assimilation system that arise from nonlinear interaction between the diurnal tide and the westward traveling quasi 2 day wave. The process yields a westward traveling "sum" wave with zonal wave number 4 and a period of 16 h, and an eastward traveling "difference" wave with zonal wave number 2 and a period of 2 days. While the eastward 2 day wave has been reported in satellite temperatures, the westward 16 h wave lies outside the Nyquist limits of resolution of twice daily local time satellite sampling. Hourly output from a high-altitude forecast-assimilation model is used to diagnose the nonlinear quadriad. A steady state primitive equation model forced by tide-2 day wave advection is used to intepret the nonlinear wave products. The westward 16 h wave maximizes in the midlatitude winter mesosphere and behaves like an inertia-gravity wave. The nonlinearly generated component of the eastward 2 day wave maximizes at high latitudes in the lower thermosphere, and only weakly penetrates to low latitudes. The 16 h and the eastward 2 day waves are of comparable amplitude and alias to the same apparent frequency when viewed from a satellite perspective.

1. Introduction

The migrating diurnal tide (DW1) and the quasi 2 day wave (Q2DW) are two of the strongest amplitude global-scale perturbations in the mesosphere and lower thermosphere (MLT). DW1 is characterized by a diurnal period and a zonal wave number of 1 and is virtually always present in the low-latitude MLT. Typical amplitudes of DW1 meridional winds range between 35 and 75 m s^{-1} in the subtropics, with the higher values occurring during equinox and the lower values at solstice [*Wu et al.*, 2008a, 2008b]. The Q2DW is a normal mode of Earth's atmosphere that is amplified in the summer easterly (westward) jet [*Salby*, 1981]. It is a predominantly zonal wave number 3 wave with a period near 48 h. The Q2DW occurs in short bursts of intense activity following the summer solstice, attaining very strong wind amplitudes (~70 m s^{-1}) [*Wu et al.*, 1993].

Teitelbaum and Vial [1991] considered the generation of secondary planetary waves and tides due to advective forces among strong amplitude migrating tides and planetary waves. The interaction of DW1 and the Q2DW produces in theory an eastward traveling 2 day wave with a zonal wave number 2 (E2), and a westward traveling wave with a zonal wave number 4 and a period of 16 h (W4). Some observational support for this mechanism has been presented in ground- and space-based data. Spectral analysis of MLT radar winds indicate the concurrent presence of diurnal and 2 day periods with one or both of the secondary waves periods predicted by nonlinear theory [*Manson and Meek*, 1990; *Clark and Bergin*, 1997; *Beard et al.*, 1999]. *Palo et al.* [2007] and *Moudden and Forbes* [2014] have reported E2 in Thermosphere Ionosphere Mesosphere Energetics and Dynamics Sounding of the Atmosphere using Broadband Emission Radiometry (SABER) MLT temperatures during Q2DW events. *Tunbridge et al.* [2011] also documented E2 in EOS Aura Microwave Limb Sounder (MLS) temperatures.

Recently, *Nguyen et al.* [2016] examined the response of a steady state, primitive equation model with a resting background to observation-based advection between DW1 and the Q2DW. Both E2 and W4 appeared in

the model with roughly equal magnitudes in the MLT. E2 attenuated rapidly above 100 km. However, W4 horizontal wind amplitudes on the order of 10 m s^{-1} were observed well into the *E* region ionosphere. This wave therefore has the potential to drive the dynamo process and transmit variability associated with the Q2DW to higher ionospheric altitudes.

Global observations of E2 and W4 are highly desirable for confirming nonlinear processes and exploring vertical coupling. However, satellite-based analyses of E2 and W4 are limited due to undersampling of W4 and aliasing among the Q2DW and its nonlinearly generated progeny [*Tunbridge et al.*, 2011; *Moudden and Forbes*, 2014]. The Q2DW and E2 can be resolved by applying asynoptic mapping techniques to data from orbiting satellites viewing Earth at two local times per day [*Salby*, 1982]. However, W4 lies outside the Nyquist limits of resolution of these data sets and moreover aliases to the E2 signal viewed from the satellite perspective.

The goals of this study are to (1) investigate E2 and W4 in the MLT in a high-altitude operational forecast model, (2) interpret their behavior with a version of the *Nguyen et al.* [2016] model that includes observed background winds, and (3) compare W4 derived from the forecast-assimilation system with observations. Sections 2 and 3 describe the high-altitude forecast model, wave analysis, and morphology of E2 and W4. In particular, we note radically different occurrences of E2, suggesting both linear and nonlinear sources. Comparisons between assimilation and ground-based observations of the 16 h wave are also presented. In section 4 we examine the implications of the W4 presence for aliasing. Conclusions appear in section 5.

2. Data

In view of the sampling limitations of available satellite data, we turn to the Navy Operational Global Atmospheric Prediction System (NOGAPS) Advanced Level Physics High Altitude (ALPHA) Dynamics model to provide definitions of W4 and E2. NOGAPS ALPHA was developed as a prototype vertical extension of the Navy's operational-forecast model to 95 km. This vertical extension required inclusion of radiative heating and cooling rates that account for nonlocal thermodynamic equilibrium, ozone and water vapor transport and photochemistry, and nonorographic gravity wave drag [*Eckermann et al.*, 2009]. The data assimilation component of NOGAPS ALPHA is a 3-D variational system with a 6-hourly update cycle that assimilates conventional meteorological data, as well as MLS and SABER temperature, and MLS ozone and H_2O. The NOGAPS ALPHA forecast-assimilation model realistically describes the large-scale circulation below 100 km down to periods near 1 day [*Eckermann et al.*, 2009; *Coy et al.*, 2009; *Siskind et al.*, 2011; *McCormack et al.*, 2009, 2010; *Nielsen et al.*, 2010; *Stevens et al.*, 2010]. *McCormack et al.* [2010] used this model to investigate nonlinear interaction among DW1 and the Q2DW, but W4 could not be resolved.

A version of NOGAPS ALPHA was configured to be initialized by the assimilation every 6 h yet provide output on an hourly cadence [*Siskind et al.*, 2012]. Hourly NOGAPS ALPHA files are available for January–February 2005, 2006, 2008, 2010, and for all months in 2009. This product allows global definitions of diurnal and other high-frequency harmonics on a day-to-day, or at least week-to-week basis. *Lieberman et al.* [2015] demonstrated that the morphology and the short-term variability of diurnal tides compared favorably with tidal proxies derived from SABER and MLS. We will therefore utilize the hourly data set for definitions of the "parent" waves (DW1 and Q2DW) and the products of their nonlinear interaction: E2 and W4. The Q2DW, DW1, E2, and W4 are computed from NOGAPS ALPHA data as the space-time Fourier harmonics of sliding 6 day (144 h) sequences.

While E2 can be compared with other published analyses, W4 can be validated only with analyses of ground-based data collected at sufficiently high cadence. We elected to compare with data from the SKiYMETS meteor radars at Juliusruh, Germany (54.6°N,13°E), and Bear Lake Utah (42°N, 111.3°W). These systems and their measurements are described more fully by *Hocking et al.* [2001], *Day et al.* [2012], and *Stober et al.* [2012]. Briefly, meteor radars receive backscatter from ablating meteors advected by winds in the 80–100 km range. Spatially separated antennas triangulate the echo position, and Doppler velocities are least squares fitted over a 1 h averaging time to obtain horizontal wind speed and direction with a 2 km height resolution.

To interpret the structure and evolution of W4 and E2, we simulate W4 and E2 with the version of the global scale wave model (GSWM) used by *Nguyen et al.* [2016] that includes meridional gradients of zonal mean temperature ($\bar{T}$) and nonzero zonal mean zonal winds ($\bar{U}$). *Nguyen et al.* [2016] modified GSWM's source code [*Hagan et al.*, 1995] to accommodate thermal and momentum source terms arising from DW1-Q2DW interaction. Secondary wave forcing is computed from 6 day averaged NOGAPS ALPHA DW1 and Q2DW definitions.

$\bar{U}$ and $\bar{T}$ are extracted from hourly NOGAPS-ALPHA reanalysis output by zonally and temporally averaging measurements at each latitude-altitude location over 6 days. The 6 day temporal window is slid 1 day to produce a unique configuration for each day. Because the NOGAPS-ALPHA model only produces output to approximately 95 km, January climatological values from the NRL Mass Spectrometer Incoherent Scatter-90 empirical model [*Hedin*, 1996] are utilized at higher altitudes. To minimize the impact of this transition, $\bar{U}$ and $\bar{T}$ are linearly smoothed between 90 km and 100 km. The model is numerically solved for the amplitudes and phases of W4 and E2 on a 3° resolution latitude grid and 4 km resolution altitude grid spanning the surface to 400 km.

3. Results

Figure 1 shows $\bar{U}$ from NOGAPS ALPHA averaged between 11 January and 3 February 2005. The summer hemisphere is dominated by westward winds that maximize at 80 m s^{-1} near 15°S and 50 km. The winter hemisphere is characterized by eastward winds that maximize between 50 and 60 m s^{-1} near 65 km and 40°N. The zero wind line occurs between 70 and 90 km in the summer hemisphere, with the higher altitude at the high latitudes. In the winter hemisphere the zero wind line is located near 95 km. Above the wind reversal altitudes, the summer eastward winds attain higher values (~40 m s^{-1}) than the winter westward winds (~10 m s^{-1}).

Figure 2 presents latitude versus time sections of the parent waves at 13 scaled heights (~85 km) during January and February 2005. Temperature, zonal, and meridional winds are shown on the left for DW1 and for the Q2DW on the right. DW1 temperature amplitudes peak at the equator and have a nearly steady value near 6 K during January. DW1 winds maximize at subtropical latitudes and range between 10 and 18 m s^{-1} during January. However, while DW1 is always present to a degree, the Q2DW is much more episodic. There is one occurrence at the start of January and another very strong amplitude episode in late January to early February [*Siskind and McCormack*, 2014]. The Q2DW is highly asymmetric, maximizing in the summer hemisphere. We note that the strongest Q2DW amplitudes coincide with the weakest DW1 winds. This behavior was also observed in the numerical Q2DW simulations of *Chang et al.* [2011].

Figure 3 presents latitude versus time sections of W4 temperatures and winds at 13 scaled heights. W4 in general is episodic and maximizes during the buildup of the Q2DW event (11–25 January). The wave structure is highly asymmetric in latitude, with much stronger amplitudes at winter midlatitudes. Peak values are between 10–12 m s^{-1} and 4 K, roughly 1/3–1/2 those of the parent Q2DW. We note that the latitudinal structure of W4 does not resemble that of either Q2DW (which is strongest in the summer midlatitudes) or DW1 (which is symmetric about the equator).

The circulation for W4 at 13 scaled heights (~87 km) on 23 January 2005 is shown in Figure 4. For clarity, the wave is only plotted between the Greenwich meridian and 90°E or over one of its four longitude cycles. The flow has the characteristics of a westward traveling inertia-gravity wave (IGW). To understand this, consider first the region between 20°S and 20°N. At these latitudes, the primary zonal momentum balance occurs among the pressure gradient force and the wind tendency:

$$\partial u/\partial t = -\partial \Phi/\partial x.$$

Maximum accelerations are located downgradient of the geopotential maximum in Figure 4. Accordingly, the peak eastward wind tendency is located near 40°E. For a wave propagating westward, peak eastward wind values will be found 1/4 cycle upstream (i.e., to the east) of the tendency, which coincides with the geopotential peturbation minimum. Thus, westward propagating IGWs are characterized between 20°S and 20°N by an antiphase relationship among the perturbation zonal winds and geopotential.

At midlatitudes, the Coriolis force becomes comparable to the 16 h wind tendencies:

$$\partial u/\partial t \sim fv$$

and

$$\partial v/\partial t \sim -fu.$$

In the Northern Hemisphere, maximum northward (southward) acceleration occurs at the position of the westward (eastward) wind maximum. Thus, northward (southward) winds are found 1/4 cycle upstream

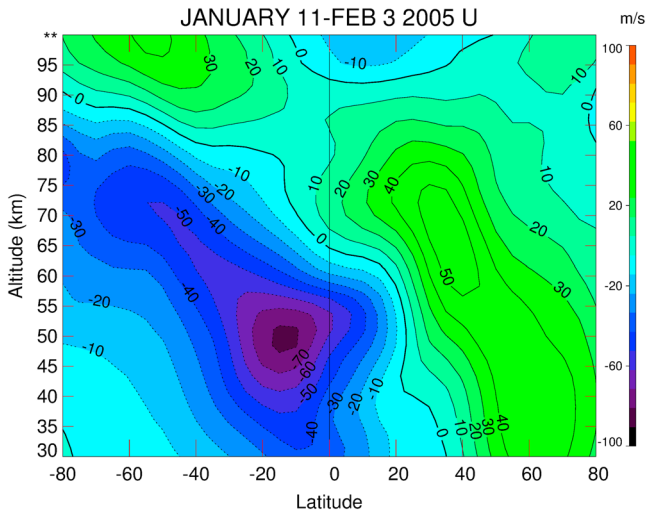

Figure 1. NOGAPS ALPHA $\bar{U}$ averaged between 11 January and 3 February 2005.

(or to the east) of the westward (eastward) wind maxima. In the Southern Hemisphere, the midlatitude wind patterns effected by the Coriolis force are reversed, with southward (northward) winds located 1/4 to the east of the westward (eastward) wind maxima.

The behaviors evinced in Figures 3 and 4 are replicated in January–February 2006, 2008, 2009, and 2010 and June–July 2009 (not shown). The global coherence of W4, its year-to-year repeatibility, and the

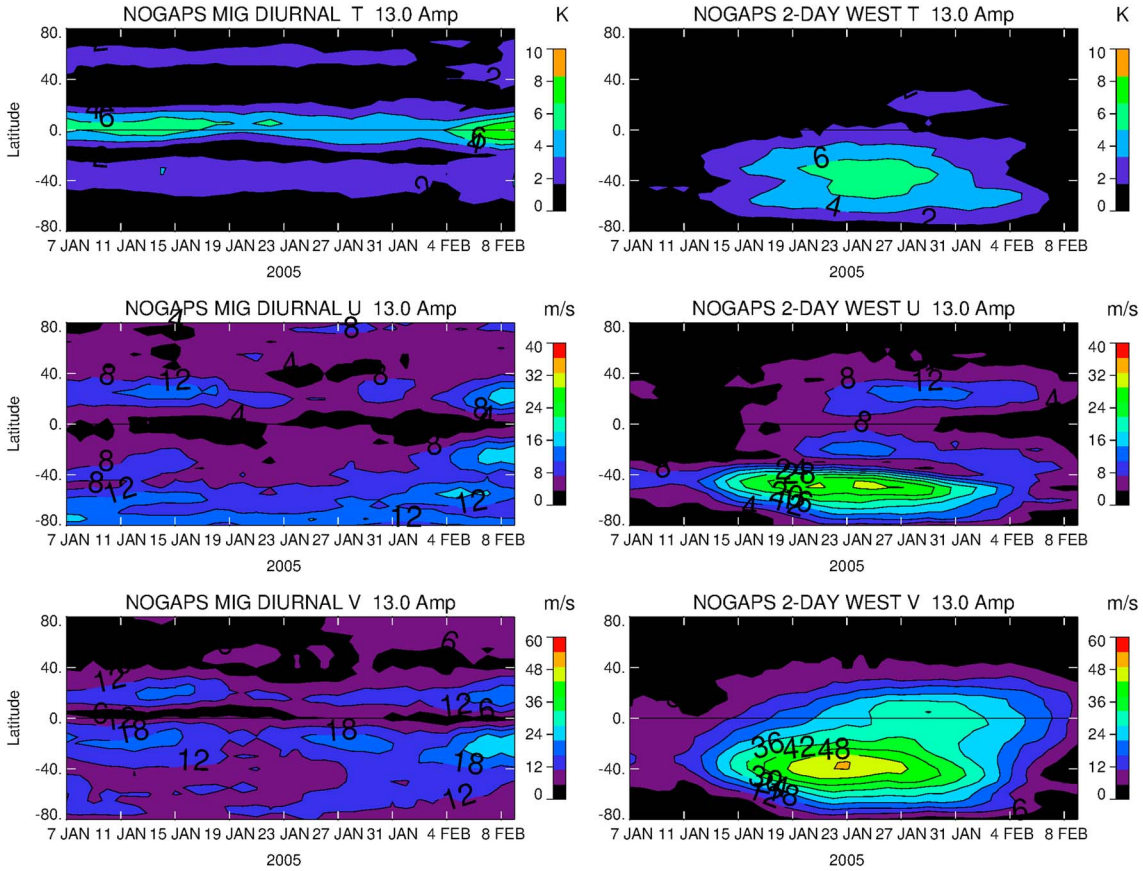

Figure 2. (left column) DW1 temperature (top), zonal (middle), and meridional (bottom) wind amplitudes at 13 scaled heights (~85 km) plotted as a function of latitude and time (January–February 2005). (right column) Same as Figure 2 (left column) but for the Q2DW.

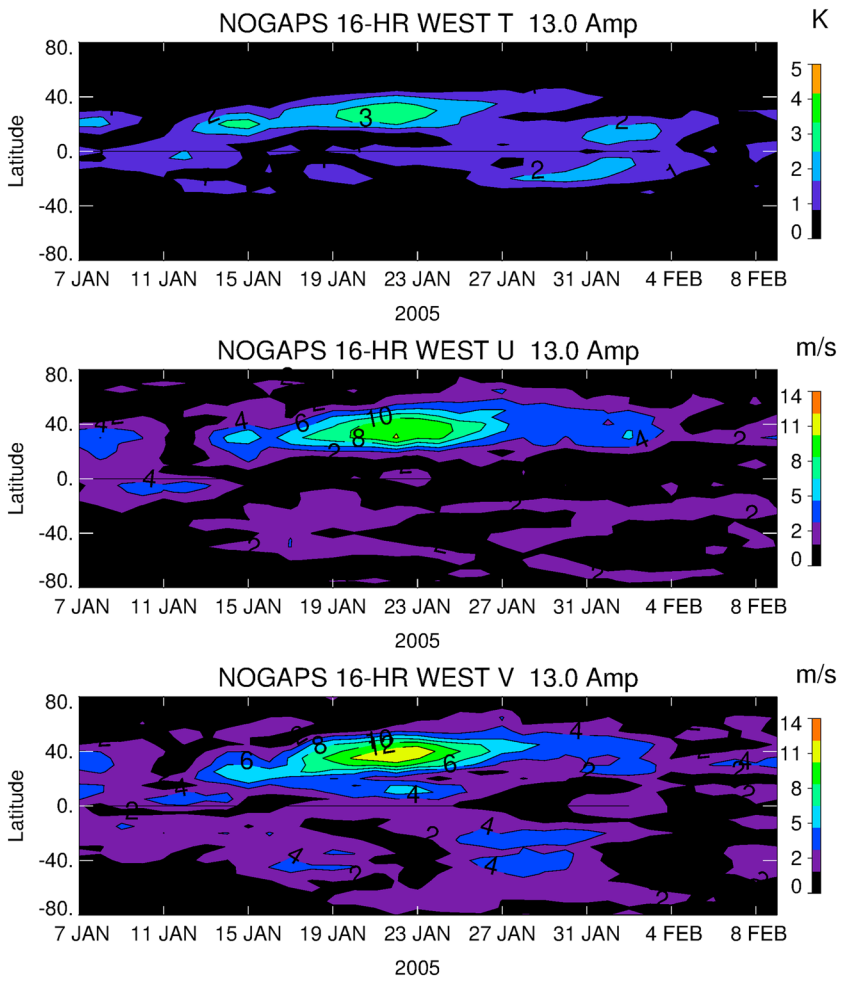

Figure 3. (top) W4 temperature amplitude at 13 scaled heights (~ 85 km) plotted as a function of latitude and time (January–February 2005). (middle) W4 zonal wind amplitude. (bottom) W4 meridional wind amplitude.

temporal coincidence with DW1 and Q2DW suggest DW1-Q2DW interaction as a possible source. To explore this idea, we examine the GSWM response to the W4 components of the momentum and heat advection among NOGAPS ALPHA DW1 and Q2DW. These numerical experiments are undertaken identically to those described in *Nguyen et al.* [2016], with the addition of NOGAPS $\bar{U}$ and the corresponding $\bar{T}$ (see section 2). The remainder of this paper focuses on the January–February 2005 event.

Figure 5 shows the evolution of the GSWM response to the W4 component of DW1-Q2DW nonlinear forcing in January 2005 at 85.5 km. The model captures the latitudinal structure, hemispheric asymmetry, and timing of W4 temperature extremely well and predicts nearly the same amplitudes. The asymmetry of the W4 winds and the overall timing is also captured very well by the model. Simulated wind amplitudes are weaker than the observed amplitudes and are sustained between 15 and 31 January, compared to the observations that show an amplitude buildup to a 23 January peak. NOGAPS ALPHA Southern Hemisphere W4 amplitudes are more muted than GSWM W4. Latitude-altitude cross sections (Figure 6) indicate that both modeled and observed W4 appear above 10 scaled heights (~70 km) and are dominant in the winter midlatitudes. Overall, Figures 3–6 convincingly suggest that W4 originates from DW1-Q2DW interaction.

It might be asked at this juncture why the W4 response maximizes in the winter hemisphere where one of the parent waves (the Q2DW) is weak. A key finding of *Nguyen et al.* [2016] is that the largest nonlinearly generated wave amplitudes are not necessarily coincident with the regions of largest parent wave or nonlinear forcing amplitudes. Although nonlinear forcing of W4 is indeed concentrated in the Q2DW region in the summer hemisphere, the process efficiently excites the gravest two vertically propagating eigenmodes (or Hough modes) of W4. These are global-scale structures that span both hemispheres. In a windless atmosphere,

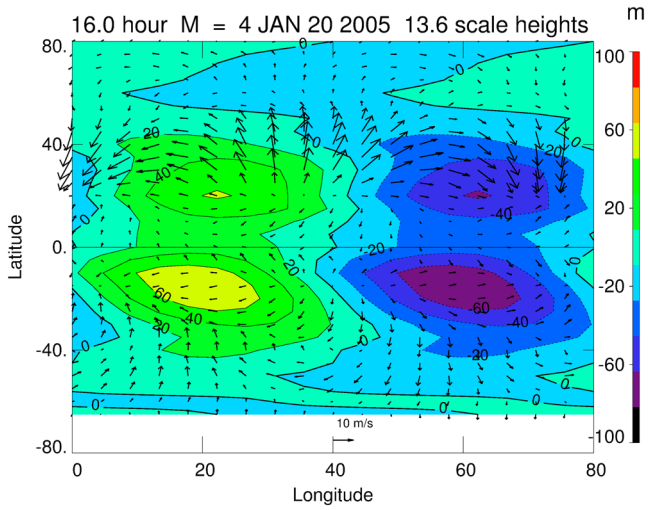

Figure 4. W4 geopotential and horizontal winds on 20 January 2005 at 13.6 scaled heights (~90 km).

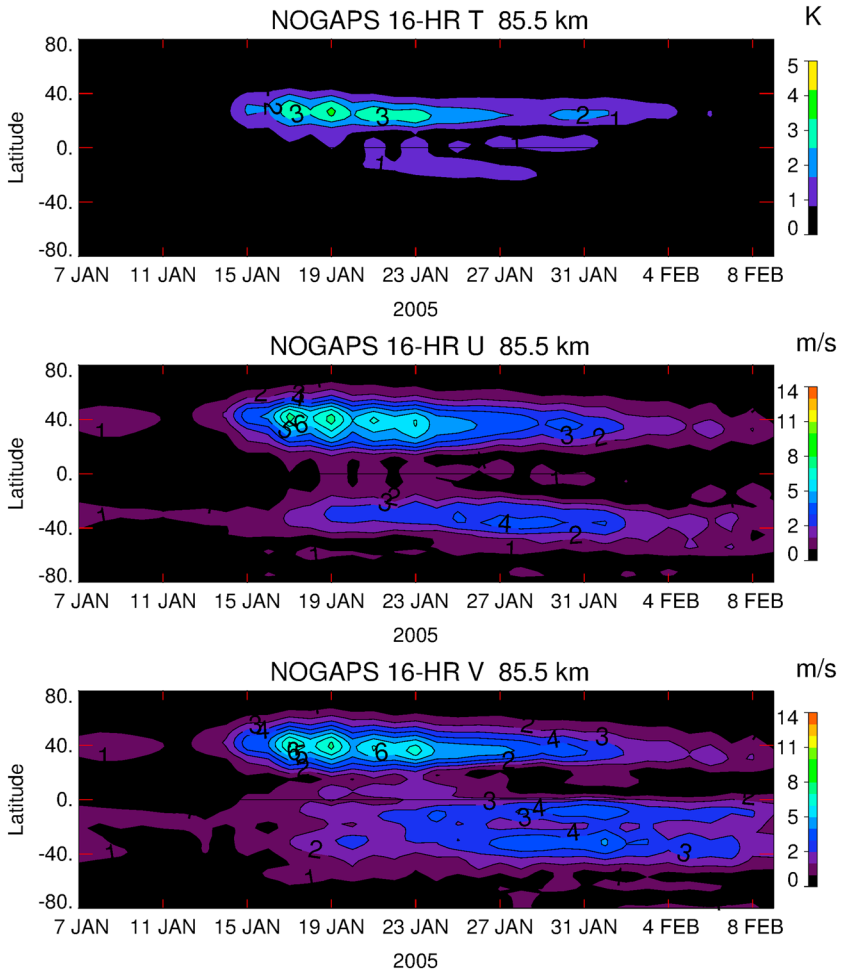

Figure 5. As in Figure 3, computed in GSWM as a response to the W4 component of DW1-Q2DW interaction.

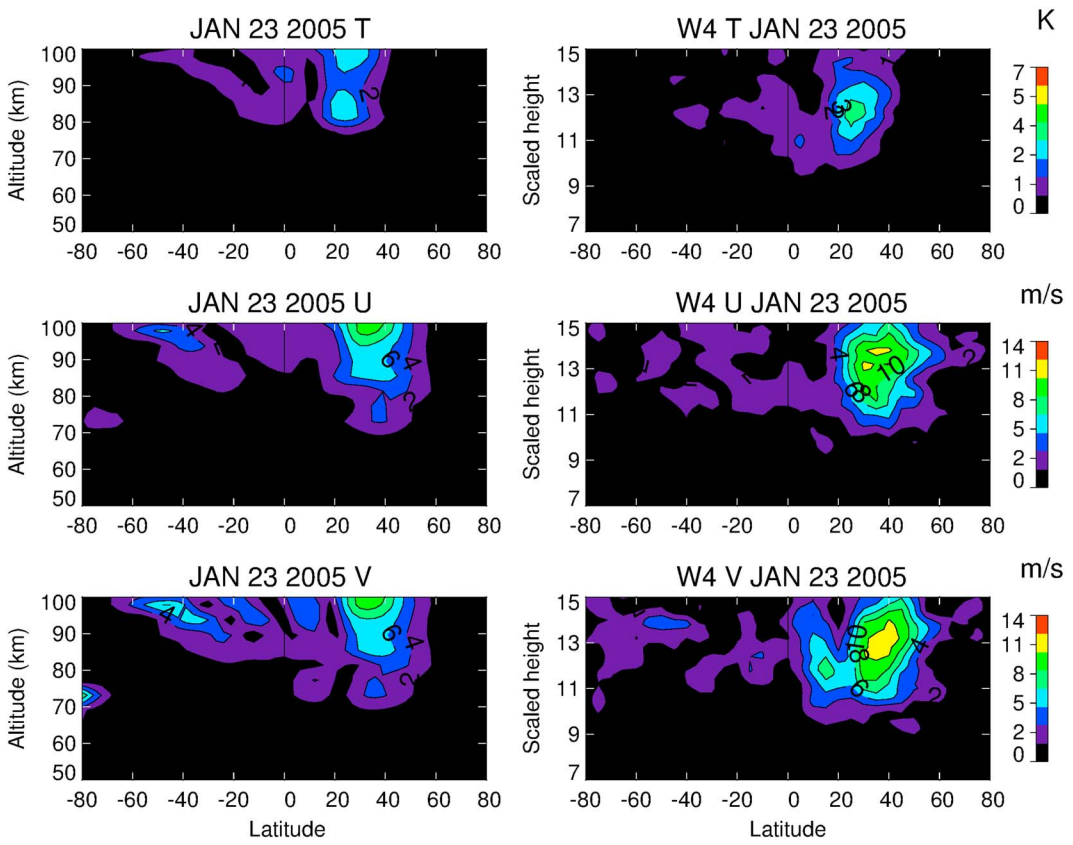

Figure 6. Latitude versus height plot of W4 amplitude centered on 23 January 2005. (top row) Temperature. (middle row) Zonal wind. (bottom row) Meridional wind. (left column) GSWM model. (right column) NOGAPS ALPHA.

the global response of W4 is dominated by a mode that is symmetric about the equator [*Nguyen et al.*, 2016]. Why then do we observe a substantially weaker W4 in the summer hemisphere during January 2005? Heuristically, this behavior reflects the properties of IGWs propagating in different wind regimes. Compared to a windless atmosphere, W4 travels at a slower zonal phase speed relative to the westward zonal mean winds ($\bar{U} < 0$) in the summer hemisphere (see Figure 1). Both the vertical wavelength and vertical group velocity of IGWs are proportional to the *intrinsic* (or background wind-relative) phase speed. As the intrinsic frequency and vertical wavelength decrease, the wave becomes increasingly prone to amplitude erosion due to transient and nonlinear phenomena such as radiative damping, instability, and turbulence [*Fritts and Alexander*, 2003]. These processes are parameterized in GSWM with diffusion and damping schemes that selectively filter oscillations with shorter wavelengths and slower group velocities [*Hagan et al.*, 1999]. Thus, vertical transmission of W4 is inhibited in westward (summer) wind regimes and promoted in the eastward background winds in the winter hemisphere.

The evolution of E2 during January–February 2005 is shown in Figure 7. At 14 scaled heights (~94 km), the strongest amplitudes are seen at low latitudes. A zonal wind maximum of 11 m s^{-1} centered on 11 January is characterized by symmetry about the equator and accompanied by a corresponding structure in temperature. These features are highly consistent with the definition of an equatorial Kelvin wave [*Lindzen and Holton*, 1968; *Andrews et al.*, 1987]. In mathematical terms, the Kelvin wave is the gravest symmetric meridional eigenfunction of an eastward and vertically propagating wave [*Longuett-Higgins*, 1967]. When $\bar{U} = 0$, this mode is characterized by Gaussian zonal wind and temperature structures centered on the equator and essentially zero meridional winds. Between 20 January and 1 February, zonal winds and temperatures have evolved into latitudinally asymmetric features, which is an indicator of a higher-order mode. This interpretation is confirmed by the appearance of meridional winds with largely symmetric structure about the equator.

The intense 9–15 January 2005 E2 episode in NOGAPS ALPHA is not aligned with any Q2DW occurrences seen in Figure 2, which suggests that DW1-Q2DW interaction is not its source. This interpretation is supported

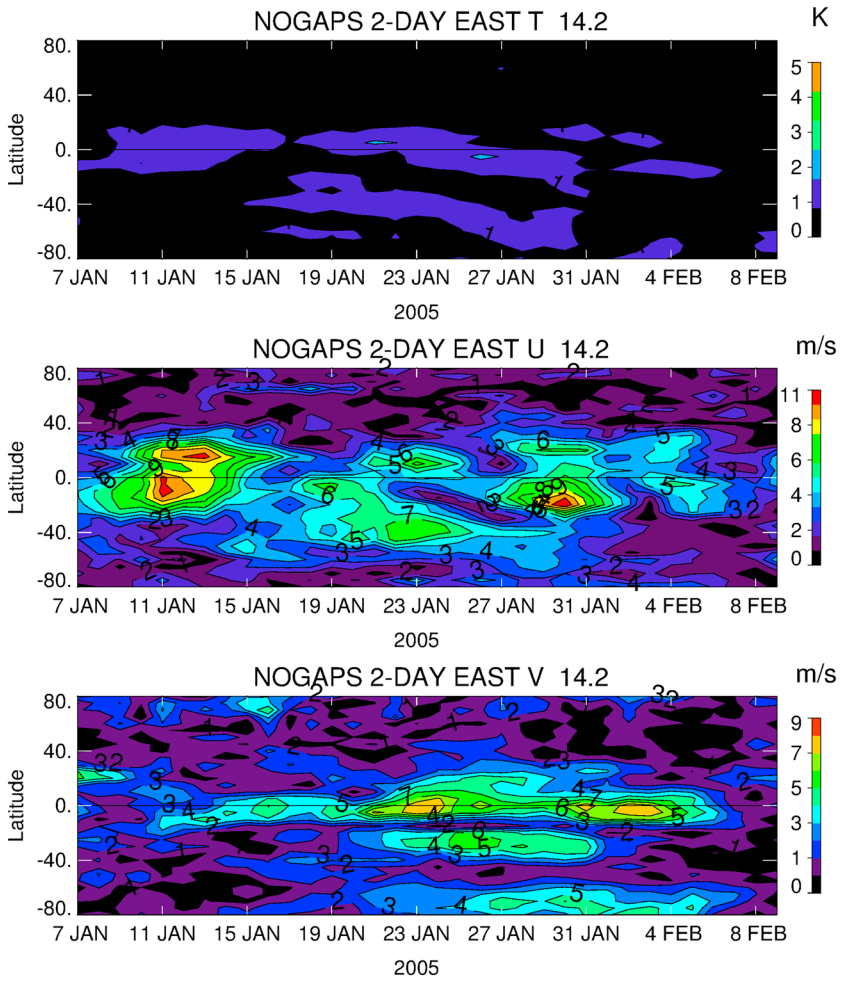

Figure 7. As in Figure 3 but for E2.

by Figure 8 showing the GSWM response to nonlinear E2 forcing. Much of the nonlinear response is confined to high summer hemisphere latitudes, with only weak penetration to equatorial latitudes. While the low-latitude features observed in NOGAP ALPHA E2 are relatively broad, the modeled E2 is narrowly concentrated in high-latitude bands. *Nguyen et al.* [2016] attribute the E2 response to the excitation of higher-order, high-latitude Hough modes with narrow latitudinal structure.

Figure 9 shows latitude-altitude cross sections of E2 on 15 January 2005 that highlight its diverse characteristics. Above 12 scaled heights (~80 km), equatorial Kelvin wave behavior is observed in NOGAPS ALPHA (right column), together with the higher-order, nonzero meridional wind mode seen at 14 scaled heights. Figure 9 (left column) shows the E2 predictions resulting from DW-Q2DW interaction. Only a small subset of the low-latitude elements of NOGAPS ALPHA E2 can be attributed to nonlinear interaction.

A high-latitude E2 is observed in the upper stratosphere and lower mesosphere that is dissociated from the tropical features and does not appear at all in the GSWM predictions. Based on its angular zonal phase speed ($\Omega/4$), and the concurrent presence of an eastward traveling zonal wave number 1 with a period of 4 days with an equivalent angular phase speed (not shown), we identify the high-latitude E2 as a member of an eastward traveling, quasi-nondispersive 4 day wave group. The 4 day wave is a ubiquitous feature in the polar winter upper stratosphere, consisting of waves 1 through at least 4 all moving with the same phase speed, such that the period of the wave "packet" is near 4 days [*Venne and Stanford*, 1979; *Allen et al.*, 1997].

The circulations associated with E2 in the lower mesosphere (10 scaled heights, or ~70 km) and the lower thermosphere (14 scaled heights) are shown in Figure 10. The mesospheric circulation is confined to latitudes poleward of 40°N and exhibits many of the characteristics of the gradient wind: cyclonic (anticyclonic)

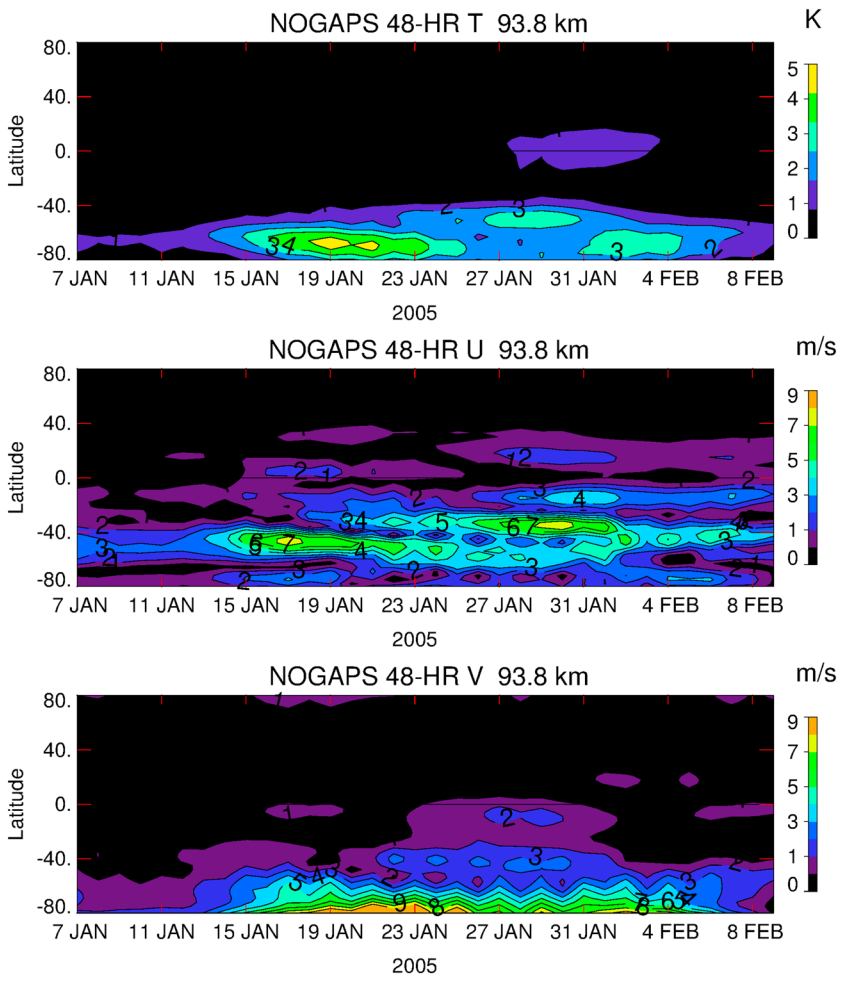

Figure 8. As in Figure 7, computed in GSWM as a response to the E2 component of DW1-Q2DW interaction.

flow around the geopotential height minimum (maximum). By contrast, at 90 km E2 is characterized by predominantly zonal flow centered about the equator. Eastward (westward) winds are in phase with positive (negative) geopotential anomalies, in accordance with Kelvin wave theory [*Andrews et al.*, 1987]. The radical differences in the high- and low-latitude circulations further support our conclusion that they are disparate phenomena.

E2 occurrences observed in NOGAPS ALPHA are consistent with analyses of global E2 amplitudes presented by *Tunbridge et al.* [2011]. However, only ground-based measurements are suitable for comparison with our W4 retrievals. To accomplish this, we apply an *S* transform [*Stockwell et al.*, 1996] to hourly meteor winds over a 3 month time segment (January-February-March). The *S* transform has a user selected localizing parameter that trades off between time and frequency resolution. We increased the localizing factor from the nominal value of 1 to 3, yielding a time window of 5 days. The output of the *S* transform is a wavelet-like representation of the field from which we extracted a single voice with a period 16 h.

Figure 11 shows 16 h winds derived from NOGAPS and observed in Bear Lake meteor radar winds (dotted) on 30 January 2009. The contributions from W4 alone (thin solid lines) are shown together with the 16 h harmonic computed in NOGAPS ALPHA at the coordinates of Bear Lake, hereafter referred to as the "total" 16 h wave (thick solid). We note first that above 90 km the phase agreement between the total NOGAPS, W4 component, and the radar 16 h waves is quite good for zonal winds. Consistency between the radar and W4 zonal wind phase extends down to 78 km. However, below 85 km the total NOGAPS 16 h phase is not as closely aligned with W4. Radar meridional wind phases also compare very favorably with W4 above 85 km, while less so

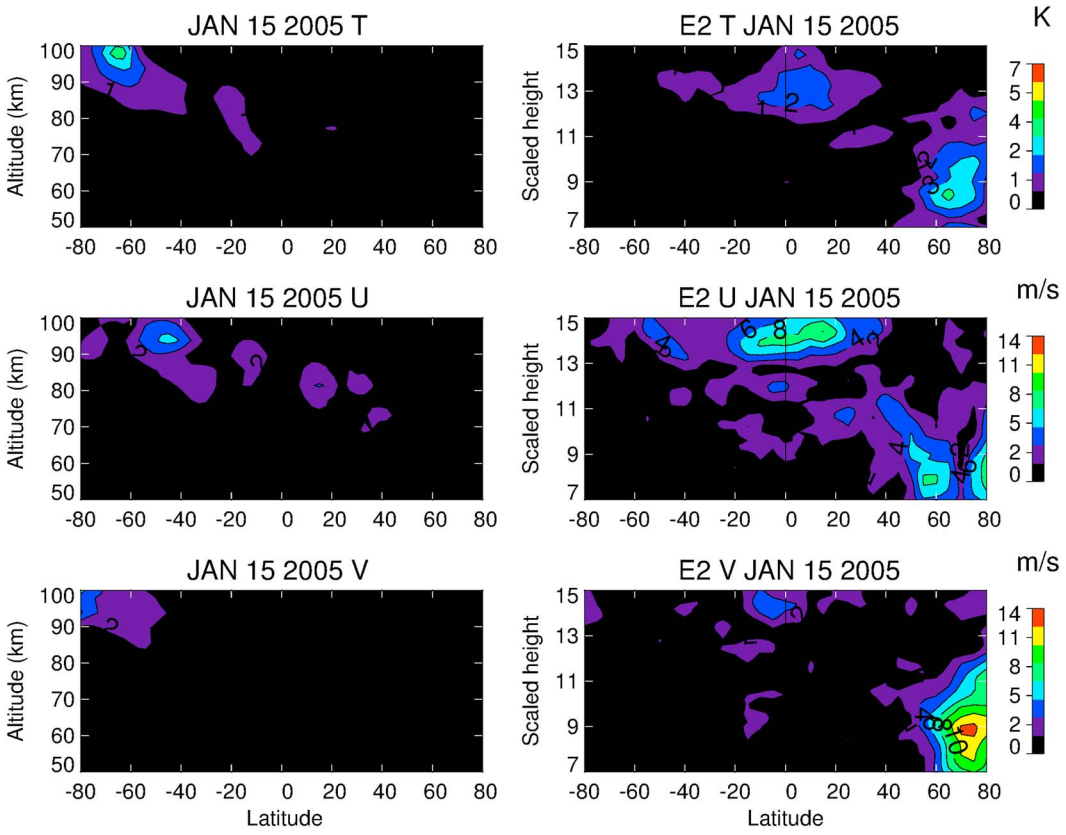

Figure 9. As in Figure 6 but for E2 on 15 January 2005.

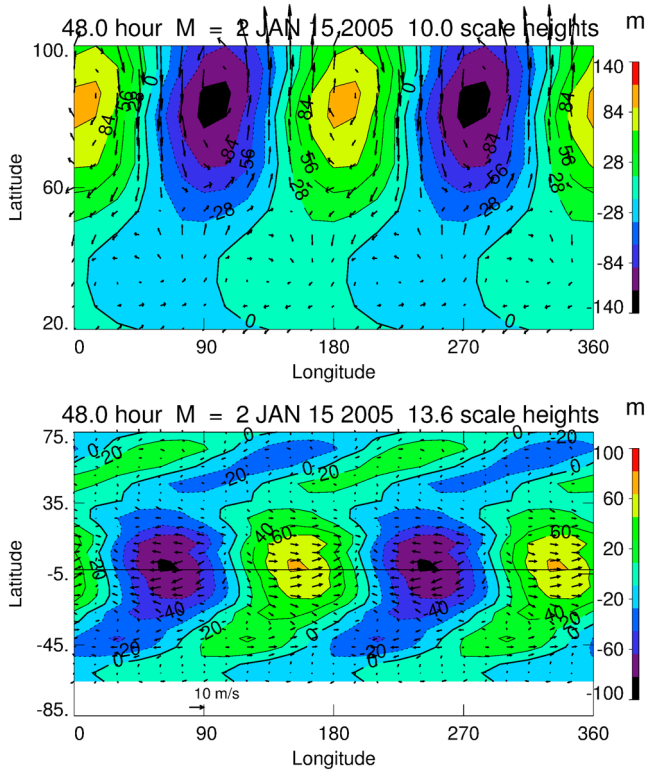

Figure 10. E2 geopotential and horizontal winds on 15 January 2005. (top) At 10 scaled heights (~70 km). (bottom) At 13.6 scaled heights (~90 km).

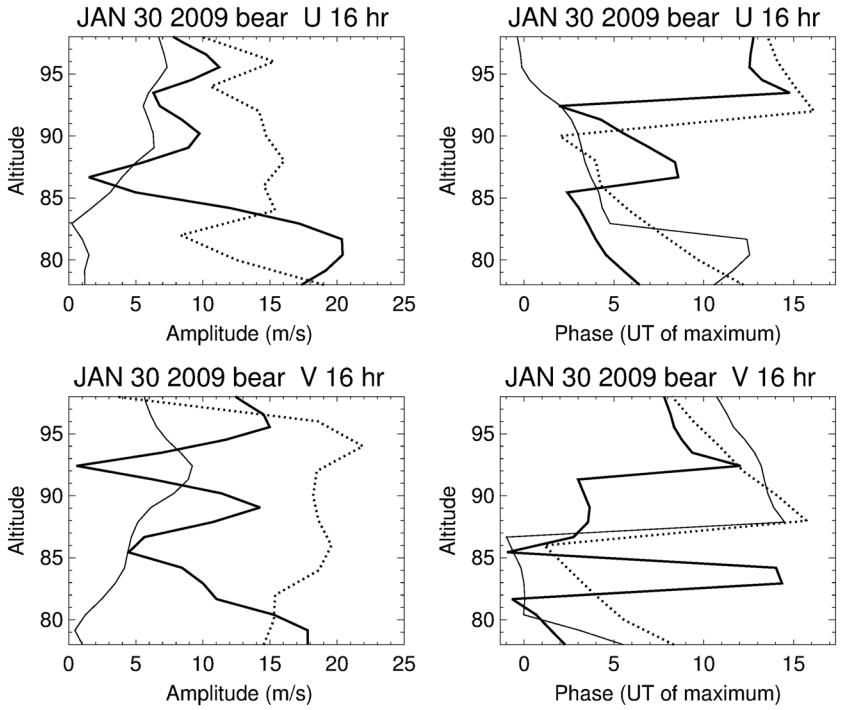

Figure 11. (top left) NOGAPS ALPHA (thick solid) and Bear Lake radar (42°N, 111.3°W) 16 h (dotted) zonal wind amplitudes on 30 January 2009. Thin solid curve is NOGAPS ALPHA W4 component. (top right) NOGAPS ALPHA (thick solid) and Bear Lake radar 16 h (dotted) zonal wind phases, in UT hour of maximum. Thin solid curve is NOGAPS ALPHA W4 component. (bottom row) Same as Figure 11 (top row) but for meridional wind.

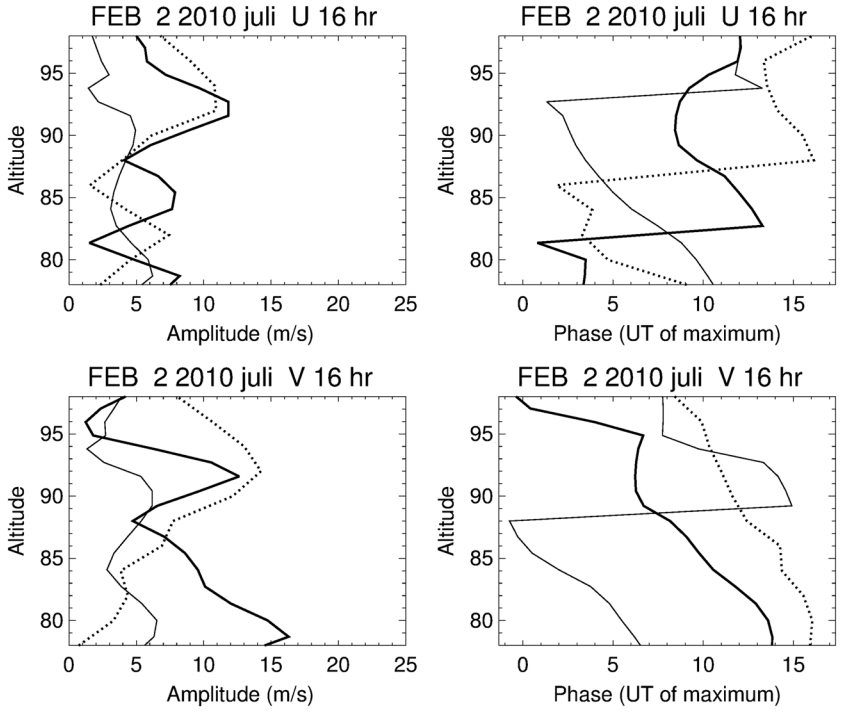

Figure 12. As in Figure 11 but for Juliusruh radar (°54.6N,13°E) on 2 February 2010.

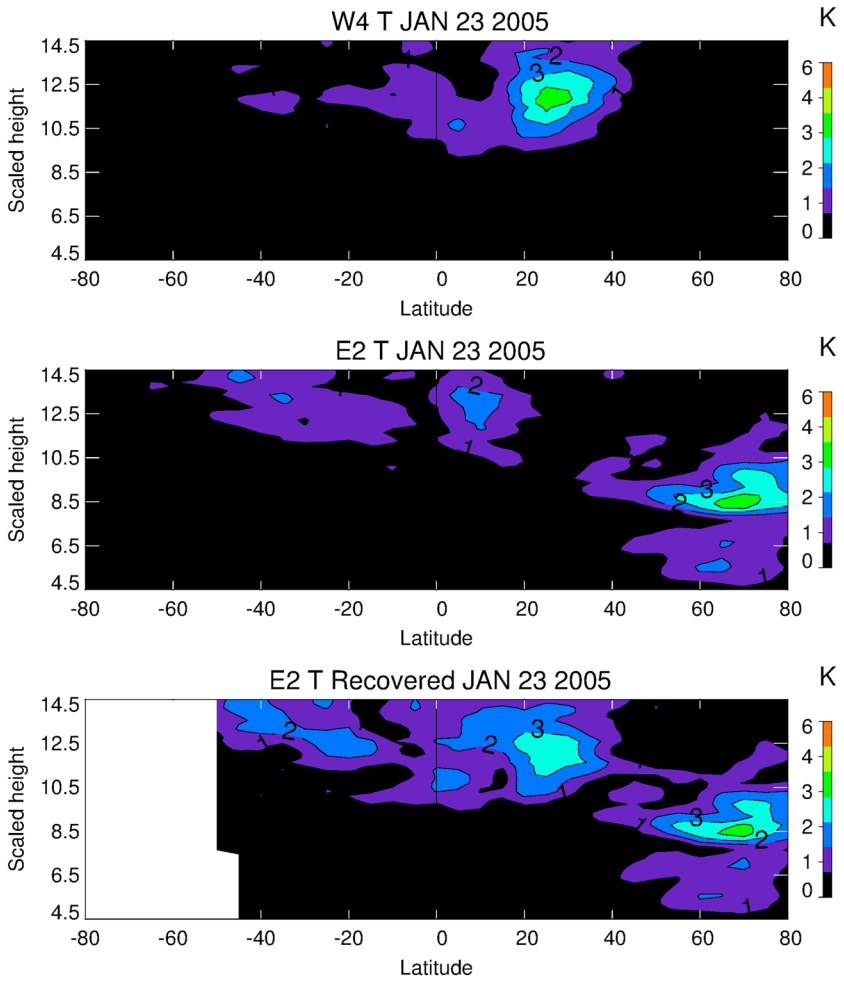

Figure 13. (top) Latitude versus scaled height plot of W4 recovered from NOGAPS ALPHA on 23 January 2005. (middle) E2 recovered from NOGAPS ALPHA on 23 January 2005. (bottom) Asynoptically mapped E2 obtained by SABER sampling NOGAPS ALPHA W4, E2, and the Q2DW.

below. The amplitude of W4 and the total 16 h zonal winds match very well above 85 km. However, the radar amplitudes exceed both NOGAPS ALPHA W4 and total 16 h amplitudes quite significantly up to about 94 km. Meridional radar wind amplitudes at Bear Lake significantly exceed both NOGAPS W4 and total 16 h winds.

At Juliusruh on 2 February 2010 (Figure 12) total 16 h zonal wind amplitudes are closely aligned with radar amplitudes above 87 km but are offset in phase by about 4 h. Meridional wind amplitudes show some similar behavior: Good 16 h NOGAPS-radar amplitude matching in a narrow region between 88 and 92 km but offset in phase. W4 and total 16 h meridional wind phases are quite consistent above 97 km.

The results of our comparisons of radar and NOGAPS ALPHA 16 h waves can therefore be summarized as mixed. The most successful comparison is that of W4 and radar 16 h winds at Bear Lake above 85 km. Both systems reveal a deep (10 km) layer of smooth phase tilt that persists despite differences in NOGAPS ALPHA and radar sampling and wind determination methods. While the phase agreements inspire confidence in the W4 interpretations, amplitude differences among NOGAPS and radars retrievals are pervasive. The reasons for these amplitude discrepancies cannot be fully determined from the observations on hand but may be related to the following circumstances: (1) The radar "footprint" is considerably smaller than that of the data input to NOGAPS ALPHA used to derive winds, leading to "smearing" of local variations at radar wind sites in the model. (2) NOGAPS ALPHA winds at radar altitudes are significantly influenced by wave drag parameterizations that may not capture the actual localized wind behavior.

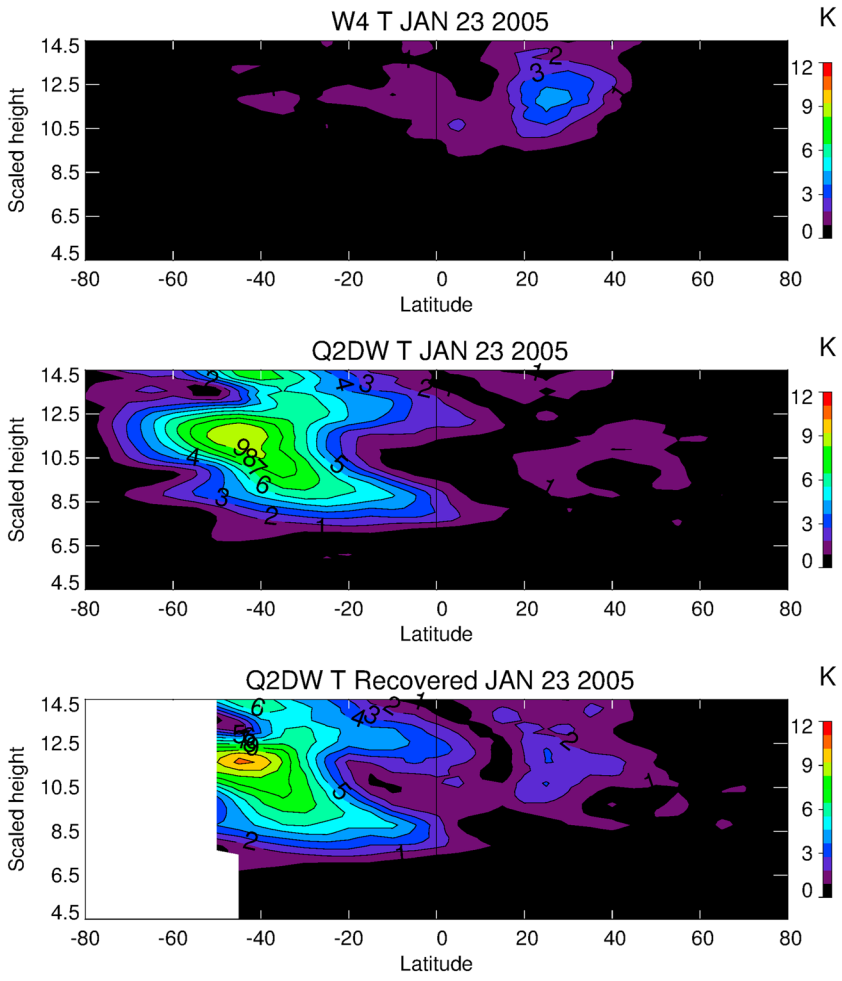

Figure 14. (top) As in Figure 13. (middle) Q2DW recovered from NOGAPS ALPHA on 23 January 2005. (bottom) Asynoptically mapped Q2DW obtained by SABER sampling NOGAPS ALPHA W4, E2, and the Q2DW.

4. Aliasing

Fast Fourier synoptic mapping (FFSM) methods are increasingly being used for satellite data analysis [*Lieberman*, 2002; *Garcia et al.*, 2005; *Palo et al.*, 2007; *Nguyen et al.*, 2016]. However, W4 lies outside the Nyquist limits of resolution of current satellite data sets [*Salby*, 1982]. Here we apply NOGAPS retrievals of E2, W4, and the Q2DW to quantify aliasing of W4 to asynoptically mapped spectra.

The FFSM method, originally developed by *Salby* [1982] and *Hayashi* [1982], computes the frequency-wave number spectrum of asynoptic measurements at each altitude-latitude grid point. Separating satellite data into ascending and descending orbital sequences at each grid point yields two independent data series that are equispaced with respect to an orbital coordinate s that is related to longitude (λ) and universal time (t) via

$$s = \frac{|\, c_0 \,|\, \lambda - t}{\sqrt{1 + c_0^2}} \tag{1}$$

c_0 is the rate at which observations precess around a latitude circle (-2π rad d^{-1} for EOS Aura). The Fourier spectra of these orbital series, denoted k_s, are related to the zonal wave numbers (m) and frequencies (σ) according to

$$k_s = \frac{|\, c_0 \,|\, m - \sigma}{\sqrt{1 + c_0^2}}. \tag{2}$$

It can be easily verified that the (m, σ) pairs for the Q2DW (3, π), E2 (2, $-\pi$), and W4 (4, 3π) all map to the satellite-viewed frequency $k_s = 2.47$ rad d^{-1}. If both ascending and descending node orbital sequences are available, the FFSM recovers the true spectrum within the Nyquist limits (m_N, σ_N) given by roughly (7, $\pm 2\pi$). E2 and the Q2DW can be separated, but if W4 is present, it will contaminate both of the retrievals.

To examine the aliasing of W4 into E2 and the Q2DW, we synthesized W4, E2, and Q2DW temperature spectra obtained from NOGAPS ALPHA at SABER latitudes, longitudes, and universal times. We then applied the FFSM to a 6 day interval centered on 23 January 2005. Figure 13 illustrates NOGAPS ALPHA W4 (top), E2 (middle), and the asynoptic retrievals of E2 (bottom). Comparing NOGAPS ALPHA and retrieved E2, we see that the presence of W4 in the pseudodata induces a significant spurious maximum in E2 at northern midlatitudes and mesospheric altitudes, where W4 maximizes. Figure 14 demonstrates that a similar imprinting of W4 occurs in the retrieval of Q2DW. The presence of W4 in the virtual data set results in a weak, spurious extension of the Q2DW temperature signature across the summer to the winter hemisphere.

5. Summary and Concluding Remarks

The goals of this study are to investigate and interpret global analyses of DW1-Q2DW interaction. We have identified W4 and E2, the products of the interaction, in 1-hourly analyses of the NOGAPS ALPHA forecast-assimilation system during six solstice periods between 2005 and 2010. Global-scale circulations of W4 in the MLT are presented here for the first time. This wave is an IGW that is coincident with the Q2DW and generally maximizes in the winter hemisphere. Wind magnitudes are about 10 m s^{-1} in the MLT. This wave is successfully simulated in a steady state primitive equation model with realistic mean winds that is forced by advection of heat and momentum between DW1 and the Q2DW. Comparisons between W4 and meteor radar winds indicate good agreement for the phase of the zonal and meridional component at Bear Lake. Although some limited amplitude agreement is observed at Juliusruh, in general, radar 16 h wind amplitudes exceed those derived from NOGAPS ALPHA.

NOGAPS ALPHA E2 analyses reveal a rich mix of tropical and high-latitude features suggesting multiple sources. E2 at low latitudes is dominated by Kelvin and higher-order meridional structures. Amplitudes of these waves far exceed those predicted by DW1-Q2DW interaction and likely have additional sources. At high summer latitudes, E2 is characterized by latitudinally narrow structure that corresponds to higher-order eigenmodes of E2. This behavior is very consistent with our model of DW1-Q2DW interaction. We also identified E2 at high latitudes in the winter stratopause and lower mesosphere. This oscillation travels with the zonal phase speed of the 4 day wave group and is unrelated to DW1-Q2DW interaction.

We examined the aliasing of W4 to E2 and Q2DW spectra mapped via asynoptic methods applied to twice daily local time satellite sampling. W4 induces spurious midlatitude signatures in E2 that have the same magnitude as the true E2. W4 also contaminates Q2DW retrievals, but these effects are weak relative to the strong amplitude of the Q2DW.

Acknowledgments

NOGAPS ALPHA hourly data are archived at NRL and available via anonymous ftp to map.nrl.navy.mil. Radar wind profiles presented in Figures 11 and 12 are available from the authors upon request. This research was supported by NASA contract NNX14AB15G and JPL subcontract 1483557. Work at the Jet Propulsion Laboratory, California Institute of Technology was performed under contract with NASA. The Juliusruh meteor radar wind analysis is supported by the WATILA grant. Portions of the work carried out by RSL were supported while serving at the National Science Foundation. Any opinion, findings and conclusions, or recommendations expressed in this publication are those of the authors and do not necessarily reflect the views of the National Science Foundation.

References

Allen, D. R., et al. (1997), The 4-day wave as observed from the Upper Atmosphere Research Satellite Microwave Limb Sounder, *J. Atmos. Sci.*, *54*, 420–434.

Andrews, D. G., J. R. Holton, and C. B. Leovy (1987), *Middle Atmosphere Dynamics*, Academic Press, Orlando, Fla.

Beard, A. G., N. J. Mitchell, P. J. S. Williams, and M. Kunitake (1999), Non-linear interactions between tides and planetary waves resulting in periodic tidal variability, *J. Atmos. Sol. Terr. Phys.*, *61*, 363–376.

Chang, L. C., S. E. Palo, and H.-L. Liu (2011), Short-term variability in the migrating diurnal tide caused by interactions with the quasi 2 day wave, *J. Geophys. Res.*, *116*, D12112, doi:10.1029/2010JD014996.

Clark, R. R., and J. S. Bergin (1997), Bispectral analysis of mesosphere winds, *J. Atmos. Sol. Terr. Phys.*, *59*(6), 629–639.

Coy, L., S. Eckermann, and K. Hoppel (2009), Planetary wave breaking and tropospheric forcing as seen in the stratospheric sudden warming of 2006, *J. Atmos. Sci.*, *66*, 495–507.

Day, K. A., M. J. Taylor, and N. J. Mitchell (2012), Mean winds, temperatures and the 16- and 5-day planetary waves in the mesosphere and lower thermosphere over Bear Lake Observatory (42°N, 111°W), *Atmos. Chem. Phys.*, *12*, 1571–1585.

Eckermann, S. D., K. W. Hoppel, L. Coy, J. P. McCormack, D. E. Siskind, K. Nielsen, A. Kochenash, M. H. Stevens, C. R. Englert, and M. Hervig (2009), High-altitude Data Assimilation System experiments for the northern summer mesosphere season of 2007, *J. Atmos. Sol. Terr. Phys.*, *71*, 531–551.

Fritts, D. C., and M. J. Alexander (2003), Gravity wave dynamics and effects in the middle atmosphere, *Rev. Geophys.*, *41*(1), 1–41.

Garcia, R. R., R. S. Lieberman, J. R. Russell, and M. G. Mlynczak (2005), Large-scale waves in the mesosphere and lower thermosphere observed by SABER, *J. Atmos. Sci.*, *62*, 4384–4399.

Hagan, M. E., J. M. Forbes, and F. Vial (1995), On modeling migrating solar tides, *Geophys. Res. Lett.*, *22*, 893–896.

Hagan, M. E., M. D. Burrage, J. M. Forbes, J. Hackney, W. J. Randel, and X. Zhang (1999), GSWM-98: Results for migrating solar tides, *J. Geophys. Res.*, *104*, 6813–6827.

Hayashi, Y. (1982), Space-time spectral analysis and its applications to atmospheric waves, *J. Meteorol. Soc. Jpn.*, *60*, 156–171.
Hedin, A. E. (1996), Extension of the MSIS thermosphere model into the middle and lower atmosphere, *J. Geophys. Res.*, *96*(A2), 1159–1172.
Hocking, W. K., B. Fuller, and B. Vandepeer (2001), Real-time determination of meteor-related parameters utilizing modern digital technology, *J. Atmos. Sol. Terr. Phys.*, *63*, 155–169.
Lieberman, R. S. (2002), Eliassen-Palm fluxes of the two-day wave, *2846-2861*, *corrigendum*, *59*, 2625–2627.
Lieberman, R. S., D. M. Riggin, D. A. Ortland, J. Oberheide, and D. E. Siskind (2015), Global observations and modeling of nonmigrating diurnal tides generated by tide-planetary wave interactions, *J. Geophys. Res. Atmos.*, *120*, 11,419–11,437, doi:10.1002/2015JD023739.
Lindzen, R. S., and J. Holton (1968), A note on kelvin waves in the atmosphere, *Mon. Weather Rev.*, *96*, 385–386.
Longuett-Higgins, M. S. (1967), The eigenfunctions of Laplace's tidal equations over a sphere, *Philos. Trans. R. Soc., A269*, 511–607.
Manson, A. H., and C. Meek (1990), Long-period (8–10 h) wind oscillations in the upper middle atmosphere at Saskatoon (52°N): Evidence for non-linear tidal effects, *Planet. Space Sci.*, *38*, 1431–1441.
McCormack, J. P., L. Coy, and K. W. Hoppel (2009), Evolution of the quasi 2-day wave during January 2006, *J. Geophys. Res.*, *114*, D20115, doi:10.1029/2009JD012239.
McCormack, J. P., S. D. Eckermann, K. W. Hoppel, and R. A. Vincent (2010), Amplification of the quasi-two day wave through nonlinear interaction with the migrating diurnal tide, *Geophys. Res. Lett.*, *37*, L16810, doi:10.1029/2010GL043906.
Moudden, Y., and J. M. Forbes (2014), Quasi-two-day wave structure, interannual variability, and tidal interactions during the 2002-2011 decade, *J. Geophys. Res. Space Physics*, *119*, 2241–2260, doi:10.1002/2013JD020563.
Nguyen, V. A., S. E. Palo, R. S. Lieberman, J. M. Forbes, and D. A. Ortland (2016), Generation of secondary waves arising from nonlinear interaction between the quasi two-day wave and the migrating diurnal tide, *J. Geophys. Res. Atmos.*, *121*, 7762–7780, doi:10.1029/2016JD024794.
Nielsen, K., D. E. Siskind, S. D. Eckermann, K. W. Hoppel, L. Coy, J. P. McCormack, S. Benze, C. E. Randall, and M. E. Hervig (2010), Seasonal variation of the quasi 5 day planetary wave: Causes and consequences for polar mesospheric cloud variability in 2007, *J. Geophys. Res.*, *115*, D18111, doi:10.1029/2009JD012676.
Palo, S. E., J. M. Forbes, X. Zhang, J. M. Russell, and M. G. Mlynczak (2007), An eastward propagating two-day wave: Evidence for nonlinear planetary wave and tidal coupling in the mesosphere and lower thermosphere, *Geophys. Res. Lett.*, *34*, L07807, doi:10.1029/2006GL027728.
Salby, M. L. (1981), The 2-day wave in the middle atmosphere: Observations and theory, *J. Geophys. Res.*, *86*, 9654–9660.
Salby, M. L. (1982), Sampling theory for asynoptic satellite observations. Part I: Space-time spectra, resolution, and aliasing, *J. Atmos. Sci.*, *39*, 2577–2601.
Siskind, D. E., and J. P. McCormack (2014), Summer mesospheric warmings and the quasi 2 day wave, *Geophys. Res. Lett.*, *41*, 717–722, doi:10.1002/2013GL058875.
Siskind, D. E., M. H. Stevens, M. Hervig, F. Sassi, K. Hoppel, C. R. Englert, and A. J. Kochenash (2011), Consenquences of recent Southern Hemisphere winter variability on polar mesospheric clouds, *J. Atmos. Sol. Terr. Phys.*, *73*, 2013–2021, doi:10.1016/j.jastp.2011.06.014.
Siskind, D. E., D. P. Drob, J. T. Emmert, M. H. Stevens, P. E. Sheese, E. J. Llewellyn, M. E. Hervig, R. Niciejewski, and A. J. Kochenash (2012), Linkages between the cold summer mesopause and thermospheric zonal mean circulation, *Geophys. Res. Lett.*, *39*, L01804, doi:10.1029/2011GL050196.
Stevens, M. H., et al. (2010), Tidally induced variations of polar mesospheric cloud altitudes and ice water content using a data assimilation system, *J. Geophys. Res.*, *115*, D18209, doi:10.1029/2009JD013225.
Stober, G., C. Jacobi, V. Matthias, P. Hoffmann, and M. Gerding (2012), Neutral air density variations during strong planetary wave activity in the mesopause region derived from meteor radar observations, *J. Atmos. Sol. Terr. Phys.*, *74*, 55–63.
Stockwell, R. G., L. Mansinha, and R. P. Lowe (1996), Localization of the complex spectrum: The S transform, *IEEE Trans. Signal Process.*, *44*, 998–1001.
Teitelbaum, H., and F. Vial (1991), On tidal variability induced by nonlinear interaction with planetary waves, *J. Geophys. Res.*, *96*, 14,169–14,178.
Tunbridge, V. M., D. J. Sandford, and N. J. Mitchell (2011), Zonal wave numbers of the summertime 2 day planetary wave observed in the mesosphere by EOS Aura Microwave Limb Sounder, *J. Geophys. Res.*, *116*, D11103, doi:10.1029/2010JD014567.
Venne, D. E., and J. L. Stanford (1979), Observations of a 4-day temperature wave in the polar winter stratosphere, *J. Atmos. Sci.*, *36*, 2016–2019.
Wu, D. L., P. B. Hays, W. R. Skinner, A. R. Marshall, M. D. Burrage, R. S. Lieberman, and D. A. Ortland (1993), Observations of the quasi 2-day wave from the high resolution Doppler imager, *Geophys. Res. Lett.*, *20*, 2853–2856.
Wu, Q., D. A. Ortland, T. L. Killeen, R. G. Roble, M. E. Hagan, H.-L. Liu, S. C. Solomon, J. Xu, W. R. Skinner, and R. J. Niciejewski (2008a), Global distribution and interannual variations of mesospheric and lower thermospheric neutral wind diurnal tide: 1. Migrating tide, *J. Geophys. Res.*, *113*, A05308, doi:10.1029/2007JA012542.
Wu, Q., D. A. Ortland, T. L. Killeen, R. G. Roble, M. E. Hagan, H.-L. Liu, S. C. Solomon, J. Xu, W. R. Skinner, and R. J. Niciejewski (2008b), Global distribution and interannual variations of mesospheric and lower thermospheric neutral wind diurnal tide: 1. Nonmigrating tide, *J. Geophys. Res.*, *113*, A05309, doi:10.1029/2007JA012543.